Nonlinear Robust Bias Observer for MEMS Gyros Using Noninertial Attitude Sensor Measurement

Ning Tang, Jieling Chang, Lingling Wang, Li Fu, *Member, IEEE*, Konstantin A. Neusypin, Maria S. Selezneva, and Linping Peng

***Abstract*—In robotic applications, the dynamics sensitivities of commercial-grade micro-electro-mechanical system (MEMS) gyros often exhibit uncertainties that cannot be accurately modeled by linear drift. To address the estimation of these uncertain biases, we propose a novel nonlinear robust bias observer (NRBO) in this article. Unlike existing nonlinear observers for attitude and gyro bias, our proposed method incorporates a dynamics-sensitive gyro bias estimation approach, achieved through the synthesis of the attitude-angular rate nonlinear dynamic coupling (AARNDC) term and the attitude-linear coupling (ALC) term. We highlight the potential advantages of our proposed method, including the asymptotic stability of the NRBO and its robustness against MEMS gyro bias instability, enabled by a rational design of the AARNDC and ALC terms. In addition to gyro bias estimation, we present the attitude estimation within the NRBO framework. Field experimental results, conducted with a cable-driven parallel robot, demonstrate the robustness of the proposed NRBO against bias instability measurement noise. Moreover, the results highlight its superior accuracy when compared with the invariant extended Kalman filter and nonlinear navigation observer methods.**

***Index Terms*—Cable-driven parallel robot, invariant extended Kalman filter (IEKF), noninertial attitude measurement, nonlinear robust bias observer (NRBO), uncertain bias estimation.**

I. Introduction

MICRO-ELECTRO-MECHANICAL system (MEMS)-based integrated navigation systems, which fuse information from MEMS-based inertial measurement units (IMUs) and external auxiliary sensors (e.g., GPS receivers, visual sensors, etc.), are extensively applied for attitude and position measurement of various vehicles (e.g., land vehicles, robots, UAVs, etc.) [1]. In low-cost applications, the accuracy of industry-grade MEMS-based integrated navigation systems is constrained by the bias errors in the MEMS gyro outputs. The random errors in MEMS gyro biases contain large run-to-run bias and environmental coupling errors [2]. When the external auxiliary information fails, these random errors will lead to a rapid degradation of the accuracy of the MEMS-based integrated navigation system. Therefore, online correction of MEMS gyro biases becomes crucial to improve the reliability and practicality of the MEMS-based integrated navigation system in low-cost applications [3].

Kalman filter-based methods are one of the widely used online correction methods for MEMS gyro biases. In these methods, a linear dynamic model of the MEMS gyro biases and their noise characteristics are assumed to be known, and stochastic filtering methods, such as nonlinear Kalman filtering, are applied to achieve online estimation and correction of the gyro biases using external auxiliary information. Qiu et al. [4] proposed an unscented quaternion estimator with measurement loss by establishing the Bernoulli random variable of the attitude estimation system model. Ding et al. [5] presented a robust attitude and gyro bias estimation algorithm based on a two-step measurement update Kalman filtering strategy. However, Kalman filter-based methods are limited by the dynamics of vehicles and the task trajectory, which makes it difficult to consistently guarantee the observability of the MEMS gyro biases [6]. Moreover, when the linear model of MEMS gyro biases and the measurement

Manuscript received 4 August 2023; revised 22 October 2023; accepted 31 October 2023. Recommended by Technical Editor S. Baldi and Senior Editor K. J. Kyriakopoulos. This work was supported in part by the National Natural Science Foundation of China under Grant 61773037, in part by the Beihang Virtual Simulation First-class Course Project under Grant 42020200, in part by the Natural Science Foundation of Beijing, China under Grant 1202018, and in part by the Component's digital transformation methods' fundamental research for micro and nanosystems of Russia under Grant #0705-2020-0041. *(Ning Tang and Jieling Chang are co-first authors.) (Corresponding author: Li Fu.)*

Ning Tang is with the School of Automation Science and Electrical Engineering, Beihang University, Beijing 100191, China, and also with the Faculty of Computer Science and Control Systems, Bauman Moscow State Technical University, 105005 Moscow, Russia (e-mail: tangning@buaa.edu.cn).

Jieling Chang is with the School of Automation Science and Electrical Engineering, Beihang University, Beijing 100191, China (e-mail: changjl@buaa.edu.cn).

Lingling Wang and Li Fu are with the National (Virtual Simulation) Experimental Teaching Demonstration Center of Mechanical and Control Engineering, Beihang University, Beijing 100191, China (e-mail: wangling0908@buaa.edu.cn; 06532@buaa.edu.cn).

Konstantin A. Neusypin and Maria S. Selezneva are with the Faculty of Computer Science and Control Systems, Bauman Moscow State Technical University, 105005 Moscow, Russia (e-mail: neusipin@bmstu.ru; ms.selezneva@bmstu.ru).

Linping Peng is with the School of Mathematics and System Sciences, Beihang University, Beijing 100191, China (e-mail: penglp@buaa.edu.cn).

Color versions of one or more figures in this article are available at https://doi.org/10.1109/TMECH.2023.3330908.

Digital Object Identifier 10.1109/TMECH.2023.3330908

noise characteristics are not accurate, it is difficult to obtain satisfactory results for online correction of gyro biases [7].

In recent years, nonlinear observers have been introduced into attitude estimation and online correction of MEMS gyro biases to address the issues of inaccurate measurement noise characteristics and inferior interference immunity associated with Kalman filter-based methods. These nonlinear observers offer advantages, such as simplicity, robustness, and chattering avoidance, in the estimation of unmodeled dynamics [8]. For example, Keighobadi et al. [9] presented a novel immersion and invariance observer for attitude-heading reference systems in urban vehicular applications. Their proposed method outperforms the extended Kalman filter in various aspects, including faster convergence time, improved attitude estimation accuracy, and enhanced computational efficiency. Reis et al. [10] designed a nonlinear observer to obtain simultaneous estimation of the attitude, Earth's spin vector, and sensor biases via the Lagrangian method. Bjørne et al. [11] proposed a semiglobally stable nonlinear observer that implemented gyro bias and attitude estimation with visual orientation and velocity measurements. Tong et al. [12] proposed a quaternion-based hybrid observer scheme to expand the stability domain and accelerate the convergence of the observer. Under the assumption that the inertial attitude errors were small, Barrau et al. [13] proposed an invariant extended Kalman filter (IEKF) as a local stable attitude and gyro bias observer. Berkane et al. [14] developed a nonlinear navigation observer (NNO), which guaranteed semiglobal exponential stability, and the observability of the observer has been analyzed. It has been shown that the nonlinear observer-based gyro bias correction methods have the advantages of low computational complexity, Lyapunov stability, and robustness to uncertain disturbances under the constraints of a known dynamic linear model of MEMS gyro biases, high-precision observation information, and specific flight trajectory [15]. However, Wang et al. [16] pointed out that the characteristics of the dynamics-sensitive MEMS gyro biases are hard to be described by a specific linear model in practical applications. To the best of authors' knowledge, nonlinear observer-based bias correction methods in the case of an unknown dynamic model of MEMS gyro bias remain undiscussed.

Considering the difficulty to derive the dynamic nonlinear model and measurement noise characteristics of MEMS gyro biases in practical applications, we propose a nonlinear robust bias observer (NRBO) for MEMS gyros using noninertial attitude measurements, inspired by the synergetic control theory [17]. The noninertial attitude measurements can be generated from visual navigation systems [11], magnetic, angular rate, and gravity sensors [5], or GPS [18]. The NRBO consists of two parts: gyro bias estimation and attitude estimation. In the part of gyro bias estimation, the quaternion-based attitude estimation and the MEMS gyro outputs are fed into the feedforward loop to estimate the attitude-linear coupling (ALC) term. The amplification gain of this loop is designed to ensure that the NRBO is robust to the MEMS gyro bias instability. Then, the attitude-angular rate nonlinear dynamic coupling (AARNDC) term is evaluated from the first-order nonlinear feedback loop. The dynamics-sensitive gyro biases can be estimated by subtracting the AARNDC term from the ALC term. In the part of attitude estimation, the estimated gyro biases are applied to online correct the MEMS gyro outputs in order to further improve the accuracy of attitude estimation. In this article, the design of NRBO is described in detail and its stability is demonstrated.

The rest of this article is organized as follows. In Section II, the quaternion and sensor model are introduced. In Section III, the detailed derivation and proof of the NRBO for MEMS gyros are presented. In Section IV, the gyro integrating (GI) attitudes of uncorrected and corrected gyro outputs are compared on a cable-driven parallel robot. Finally, Section V concludes this article.

II. Problem Formulation

A. Quaternion

The attitude of vehicles can be expressed as the quaternion $\mathbf{\Lambda}$ in the following, which represents the relative orientation between the body frame (b-frame) and the navigation frame (n-frame)

$$\mathbf{\Lambda} = 1 \cdot \mathbf{\Lambda}_r + \boldsymbol{I}_i^T \cdot \mathbf{\Lambda}_i \tag{1}$$

where $\mathbf{\Lambda}_r = \lambda_0$ is the real part of the quaternion, $\boldsymbol{I}_i = [\boldsymbol{i}\ \boldsymbol{j}\ \boldsymbol{k}]^T$ is the imaginary unit vector, and $\mathbf{\Lambda}_i = [\lambda_2\ \lambda_2\ \lambda_3]^T$ is the imaginary part of the quaternion. The relationship between the quaternion $\mathbf{\Lambda}$ and direction cosine matrix (DCM) $\boldsymbol{R}_1(\mathbf{\Lambda})$ is

$$\boldsymbol{R}_1(\mathbf{\Lambda}) = (\mathbf{\Lambda}_r^2 - \mathbf{\Lambda}_i^T\mathbf{\Lambda}_i)\boldsymbol{I}_3 - 2\mathbf{\Lambda}_r\mathbf{\Lambda}_i^{\times} + 2\mathbf{\Lambda}_i\mathbf{\Lambda}_i^T \tag{2}$$

where $\boldsymbol{I}_3$ is a third-order unit matrix and $\mathbf{\Lambda}_i^{\times}$ is a 3-D antisymmetric matrix determined by $\mathbf{\Lambda}_i$

$$\mathbf{\Lambda}_i^{\times} = \begin{bmatrix} 0 & -\lambda_3 & \lambda_2 \\ \lambda_3 & 0 & -\lambda_1 \\ -\lambda_2 & \lambda_1 & 0 \end{bmatrix}. \tag{3}$$

The quaternion is a four-parametric hypercomplex number. To describe the position, angular velocity, etc. in 3-D real-space with quaternions, a hypercomplex map is defined $\mathbf{\Upsilon} = H(\boldsymbol{\upsilon})$, where $H : \mathbb{R}^3 \to \mathbb{R} \times \mathbb{E}^3$, $\boldsymbol{\upsilon} = [\upsilon_x\ \upsilon_y\ \upsilon_z]^T$ is an arbitrary 3-D vector, and $\mathbf{\Upsilon} = 0 + \boldsymbol{i}\upsilon_x + \boldsymbol{j}\upsilon_y + \boldsymbol{k}\upsilon_z$ is the quaternion after the hypercomplex mapping. Also, we define a map $\boldsymbol{G} = h(\mathbf{\Gamma})$, where $h : \mathbb{R} \times \mathbb{E}^3 \to \mathbb{R}^4$, $\mathbf{\Gamma} = \tau_0 + \boldsymbol{i}\tau_1 + \boldsymbol{j}\tau_2 + \boldsymbol{k}\tau_3$ is an arbitrary quaternion and $\boldsymbol{G} = [\tau_0\ \tau_1\ \tau_2\ \tau_3]^T$ is column vector corresponding to quaternion $\mathbf{\Gamma}$. So, attitude kinematics by the Poisson equation and its representation in $\mathbb{R}^4$ are stated as

$$\dot{\mathbf{\Lambda}} = \frac{1}{2}\mathbf{\Lambda} \otimes H(\boldsymbol{\omega}_{nb}^b) \tag{4}$$

$$\dot{\boldsymbol{\lambda}} = \frac{1}{2}\boldsymbol{M}(\boldsymbol{\lambda})\mathbf{\Omega}_{nb}^b \tag{5}$$

where the symbol $\otimes$ denotes the quaternion product operator, $\boldsymbol{\omega}_{nb}^b \in \mathbb{R}^3$ is the attitude angular rate vector in b-frame with respect to n-frame, $\boldsymbol{\lambda} = h(\mathbf{\Lambda}) = [\lambda_0\ \lambda_1\ \lambda_2\ \lambda_3]^T$ is attitude quaternion vector, and $\mathbf{\Omega}_{nb}^b = h \circ H(\boldsymbol{\omega}_{nb}^b) = [0\ (\boldsymbol{\omega}_{nb}^b)^T]^T$ is the attitude angular rate quaternion vector. The symbol $\circ$ indicates a composite of functions. The attitude quaternion matrix

$\boldsymbol{M}(\boldsymbol{\lambda})$ can be expressed as

$$\boldsymbol{M}(\boldsymbol{\lambda}) = \boldsymbol{\Lambda}_r \boldsymbol{I}_4 + \begin{bmatrix} 0 & -\boldsymbol{\Lambda}_i^T \\ \boldsymbol{\Lambda}_i & \boldsymbol{\Lambda}_i^{\times} \end{bmatrix}. \tag{6}$$

Accordingly, the attitude kinematics (4) represented by the DCM can be expressed as follows [19]:

$$\dot{\boldsymbol{R}}_1 = \boldsymbol{R}_1 \left(\boldsymbol{\omega}_{nb}^b\right)^{\times}. \tag{7}$$

B. Sensor Model

The model of gyro outputs can be described as

$$\underline{\boldsymbol{\omega}}_{ib}^b = \boldsymbol{\omega}_{ib}^b + \Delta\boldsymbol{\omega}_{ib}^b \tag{8}$$

where $\underline{\boldsymbol{\omega}}_{ib}^b$ is angular rate from the three-axis gyros, $\boldsymbol{\omega}_{ib}^b$ is the instantaneous angular rate of vehicles relative to inertial space, and $\Delta\boldsymbol{\omega}_{ib}^b$ denotes the slow-varying gyro biases and noise uncertainties, whose statistical properties are unknown.

Assumption 1: Consider that MEMS gyros are generally unable to be sensitive to the angular rate of Earth rotation $\boldsymbol{\omega}_{ie}$, and are applied in a limited region, so we have $\boldsymbol{\omega}_{nb}^b \approx \boldsymbol{\omega}_{ib}^b$.

A noninertial attitude sensor measurement model can be constructed as external auxiliary information

$$\boldsymbol{\Lambda}_c = \boldsymbol{\Lambda}^{-1} \otimes \Delta\boldsymbol{\Lambda}_c \tag{9}$$

where $\boldsymbol{\Lambda}_c$ is noninertial attitude measurement quaternion and $\Delta\boldsymbol{\Lambda}_c \approx [1\ (\Delta\boldsymbol{\Psi})^T]^T$ [5], $\Delta\boldsymbol{\Psi} = [\Delta\Psi_{\mathrm{R}}\ \Delta\Psi_{\mathrm{P}}\ \Delta\Psi_{\mathrm{Y}}]^T$ denotes the measurement noise.

Assumption 2: The measurement noise $\Delta\boldsymbol{\Psi}$ is zero-mean, and there exists constant $c_1 > 0$, such that $\|\Delta\boldsymbol{\Psi}\| \le c_1$.

C. Observer Objective

Based on the Poisson equation (4), the model of gyro outputs (8), and the noninertial attitude sensor measurement model (9), NRBO is developed for the purpose of estimating the attitude and gyro bias. The designed observer incorporates the following noteworthy features.

1) Accounting for the dynamics sensitivities of gyro bias, a nonlinear estimation of gyro bias is established. Simultaneously, the estimation of the vehicle's attitude is provided based on the Poisson equation.
2) The stability of the proposed observer is established through rigorous analysis, and the observer's parameters are meticulously designed based on stability considerations. This ensures a streamlined and efficient design process.
3) Ensuring that the gyro bias estimation error meets the specified performance metrics.

III. Nonlinear Robust Bias Observer Design

Substituting the gyro outputs model (8) into the Poisson equation (4) under Assumption 1 and considering the gyro drift to be nonlinearly related to vehicles motion according to relevant studies in the last few years [20], the state equations of NRBO can be derived as follows:

$$\dot{\boldsymbol{\lambda}} = \frac{1}{2}\boldsymbol{M}(\boldsymbol{\lambda})\underline{\boldsymbol{\Omega}}_{ib}^b - \frac{1}{2}\boldsymbol{M}(\boldsymbol{\lambda})\Delta\boldsymbol{\Omega}_{ib}^b \tag{10}$$

$$\Delta\dot{\boldsymbol{\Omega}}_{ib}^b = \boldsymbol{G}(\boldsymbol{\lambda}, \boldsymbol{\Omega}_{ib}^b)\Delta\boldsymbol{\Omega}_{ib}^b \tag{11}$$

where $\Delta\boldsymbol{\Omega}_{ib}^b = h \circ H(\Delta\boldsymbol{\omega}_{ib}^b)$ is gyro bias quaternion vector, $\underline{\boldsymbol{\Omega}}_{ib}^b = h \circ H(\underline{\boldsymbol{\omega}}_{ib}^b)$ is gyro outputs quaternion vector, and $\boldsymbol{G}(\boldsymbol{\lambda}, \boldsymbol{\Omega}_{ib}^b)$ is a fourth-order real matrix. $\xi_i(\boldsymbol{G}), i = 1, \ldots, 4$ are eigenvalues of $\boldsymbol{G}(\boldsymbol{\lambda}, \boldsymbol{\Omega}_{ib}^b)$, which capture the variation of gyro bias subject to the motion state of vehicles, such as attitude and angular rate.

Assumption 3: There exist constants $c_2, c_3 > 0$, such that $\|\Delta\boldsymbol{\Omega}_{ib}^b\| \le c_2$ and $\|\xi(\boldsymbol{G})\| \le c_3$.

From (10) and (11), it can be seen that the attitude quaternion vector $\boldsymbol{\lambda}$ can be directly observed from the noninertial attitude sensor measurement (9), while the gyro bias quaternion vector $\Delta\boldsymbol{\Omega}_{ib}^b$ is indirectly observable [21]. Note that, (10) can be interpreted as a nominal model of $\boldsymbol{\lambda}$, and the uncertainties stem from both $\Delta\boldsymbol{\Lambda}_c$ and $\Delta\boldsymbol{\Omega}_{ib}^b$. Assumptions 2 and 3 establish the boundaries for these uncertainties.

A. NRBO for Estimating Only Gyro Bias

NRBO design can be accomplished by first focusing on estimating only the gyro bias $\Delta\boldsymbol{\omega}_{ib}^b$ in a simplified scenario. Here, we assume that the true attitude $\boldsymbol{\Lambda}$ is already known, inspired by the design procedure in [19] and [22]. This choice of emphasis not only holds theoretical implications but also has practical significance, since the attitude is directly observable and its estimation is relatively easier, compared with the gyro bias [21]. The method proposed in this section distinguishes our article from existing algorithms employed for gyro bias estimation. Subsequently, in the next section, we will delve into observer design on the basis of this section, encompassing both gyro bias and attitude estimation.

NRBO for the gyro bias estimation is

$$\hat{\boldsymbol{S}}(\boldsymbol{\lambda}) = -\boldsymbol{K}(\boldsymbol{\Omega}_{ib}^b)\boldsymbol{\lambda} \tag{12}$$

$$\dot{\hat{\boldsymbol{z}}} + \boldsymbol{L}(\boldsymbol{\lambda}, \boldsymbol{\Omega}_{ib}^b)\hat{\boldsymbol{z}} = \boldsymbol{u} \tag{13a}$$

$$\boldsymbol{u} = -\frac{1}{2}\boldsymbol{K}(\boldsymbol{\Omega}_{ib}^b)\boldsymbol{M}(\boldsymbol{\lambda})\underline{\boldsymbol{\Omega}}_{ib}^b + \boldsymbol{L}(\boldsymbol{\lambda}, \boldsymbol{\Omega}_{ib}^b)\hat{\boldsymbol{S}}(\boldsymbol{\lambda}) \tag{13b}$$

$$\Delta\hat{\boldsymbol{\omega}}_{ib}^b = (h \circ H)^{-1}(\Delta\hat{\boldsymbol{\Omega}}_{ib}^b) = (h \circ H)^{-1}[\hat{\boldsymbol{S}}(\boldsymbol{\lambda}) - \hat{\boldsymbol{z}}] \tag{14}$$

where $\boldsymbol{L}(\boldsymbol{\lambda}, \boldsymbol{\Omega}_{ib}^b)$ is the fourth-order feedback gain matrix, which has an eigenvalue of zero and three positive eigenvalues, $\boldsymbol{K}(\boldsymbol{\Omega}_{ib}^b)$ is the fourth-order diagonal matrix independent of $\boldsymbol{\lambda}$, $\hat{\boldsymbol{S}}(\boldsymbol{\lambda}) \in \mathbb{R}^4$ is the ALC term, $\boldsymbol{u} \in \mathbb{R}^4$ is the driving term of attitude-angular rate coupled nonlinear dynamic equation (13a), and $\hat{\boldsymbol{z}} \in \mathbb{R}^4$ denotes the AARNDC term.

Theorem 1: Consider the state variable $\Delta\boldsymbol{\Omega}_{ib}^b$ of the given nonlinear state equations (10) and (11) under Assumptions 1–3 with known $\boldsymbol{\lambda}$, the gyro bias estimation $\Delta\hat{\boldsymbol{\omega}}_{ib}^b$ can be obtained from (12)–(14).

Proof: Define the estimation error of gyro bias quaternion vector $\boldsymbol{\Xi}$ as

$$\boldsymbol{\Xi} = \Delta\boldsymbol{\Omega}_{ib}^b - \Delta\hat{\boldsymbol{\Omega}}_{ib}^b. \tag{15}$$

Results in [20] indicate that gyro bias is related to attitude and angular velocity, so it is worth taking full advantage of the angular rate quaternion $\underline{\boldsymbol{\Omega}}_{ib}^{b}$ and the attitude quaternion vector $\boldsymbol{\lambda}$ to construct $\Delta\hat{\boldsymbol{\Omega}}_{ib}^{b}$

$$\Delta\hat{\boldsymbol{\Omega}}_{ib}^{b} = \hat{\boldsymbol{S}}(\boldsymbol{\lambda}) - \hat{\boldsymbol{z}}(\underline{\boldsymbol{\Omega}}_{ib}^{b}) \tag{16}$$

where $\hat{\boldsymbol{S}} \in \mathbb{R}^4$ and $\hat{\boldsymbol{z}} \in \mathbb{R}^4$. To enable $\Delta\hat{\boldsymbol{\Omega}}_{ib}^{b}$ track on $\Delta\boldsymbol{\Omega}_{ib}^{b}$, $\hat{\boldsymbol{S}}$ and $\hat{\boldsymbol{z}}$ are presumed to be continuously differentiable inspired by the design of immersion and invariance observer [9].

Write the first-order differential equation of the estimation error of gyro bias quaternion vector $\boldsymbol{\Xi}$ using (10), (11), (15), and (16), we obtain its dynamic variation

$$\dot{\boldsymbol{\Xi}} + \boldsymbol{L}(\boldsymbol{\lambda}, \boldsymbol{\Omega}_{ib}^{b})\boldsymbol{\Xi} = \boldsymbol{B}\Delta\boldsymbol{\Omega}_{ib}^{b} + \boldsymbol{D} \tag{17}$$

where $\boldsymbol{L}(\boldsymbol{\lambda}, \boldsymbol{\Omega}_{ib}^{b})$ is a fourth-order real diagonal matrix for convenience and

$$\boldsymbol{B} = \boldsymbol{G}(\boldsymbol{\lambda}, \boldsymbol{\Omega}_{ib}^{b}) + \frac{1}{2}\frac{\partial\hat{\boldsymbol{S}}(\boldsymbol{\lambda})}{\partial\boldsymbol{\lambda}^{T}}\boldsymbol{M}(\boldsymbol{\lambda}) + \boldsymbol{L}(\boldsymbol{\lambda}, \boldsymbol{\Omega}_{ib}^{b}) \tag{18}$$

$$\boldsymbol{D} = -\frac{1}{2}\frac{\partial\hat{\boldsymbol{S}}(\boldsymbol{\lambda})}{\partial\boldsymbol{\lambda}^{T}}\boldsymbol{M}(\boldsymbol{\lambda})\underline{\boldsymbol{\Omega}}_{ib}^{b} + \dot{\hat{\boldsymbol{z}}} - \boldsymbol{L}(\boldsymbol{\lambda}, \boldsymbol{\Omega}_{ib}^{b})[\hat{\boldsymbol{S}}(\boldsymbol{\lambda}) - \hat{\boldsymbol{z}}]. \tag{19}$$

From (17), it can be seen that since $\Delta\boldsymbol{\Omega}_{ib}^{b}$ is unknown, if and only if $\boldsymbol{B} \equiv \boldsymbol{0}_{4\times4}$ and $\boldsymbol{D} \equiv \boldsymbol{0}$, the estimation error of gyro bias quaternion vector $\boldsymbol{\Xi}$ converges asymptotically to zero, i.e.,

$$\dot{\boldsymbol{\Xi}} + \boldsymbol{L}(\boldsymbol{\lambda}, \boldsymbol{\Omega}_{ib}^{b})\boldsymbol{\Xi} = \boldsymbol{0}. \tag{20}$$

The following partial differential equation can be formulated from $\boldsymbol{B} \equiv \boldsymbol{0}_{4\times4}$:

$$\frac{\partial\hat{\boldsymbol{S}}(\boldsymbol{\lambda})}{\partial\boldsymbol{\lambda}^{T}} = -2[\boldsymbol{G}(\boldsymbol{\lambda}, \boldsymbol{\Omega}_{ib}^{b}) + \boldsymbol{L}(\boldsymbol{\lambda}, \boldsymbol{\Omega}_{ib}^{b})]\boldsymbol{M}^{-1}(\boldsymbol{\lambda}). \tag{21}$$

As a convenience for the solution of partial differential equation (21), let

$$\boldsymbol{G}(\boldsymbol{\lambda}, \boldsymbol{\Omega}_{ib}^{b}) + \boldsymbol{L}(\boldsymbol{\lambda}, \boldsymbol{\Omega}_{ib}^{b}) = \frac{1}{2}\boldsymbol{K}(\boldsymbol{\Omega}_{ib}^{b})\boldsymbol{M}(\boldsymbol{\lambda}) \tag{22}$$

where $\boldsymbol{K}(\boldsymbol{\Omega}_{ib}^{b})$ is a fourth-order diagonal matrix, and its first element is 0. Since matrix $\boldsymbol{L}(\boldsymbol{\lambda}, \boldsymbol{\Omega}_{ib}^{b})$ is a diagonal matrix with the first element being 0, the first row elements of matrix $\boldsymbol{G}(\boldsymbol{\lambda}, \boldsymbol{\Omega}_{ib}^{b})$ are all zeroes. The adaptive determination of $\boldsymbol{G}(\boldsymbol{\lambda}, \boldsymbol{\Omega}_{ib}^{b})$ is achieved through the involvement of $\boldsymbol{K}(\boldsymbol{\Omega}_{ib}^{b})$, $\boldsymbol{L}(\boldsymbol{\lambda}, \boldsymbol{\Omega}_{ib}^{b})$, and $\boldsymbol{M}(\boldsymbol{\lambda})$. Specifically, $\boldsymbol{M}(\boldsymbol{\lambda})$ and $\boldsymbol{K}(\boldsymbol{\Omega}_{ib}^{b})$ exhibit dependencies on $\boldsymbol{\lambda}$ and $\boldsymbol{\Omega}_{ib}^{b}$, respectively, while $\boldsymbol{L}(\boldsymbol{\lambda}, \boldsymbol{\Omega}_{ib}^{b})$ is associated with both $\boldsymbol{\lambda}$ and $\boldsymbol{\Omega}_{ib}^{b}$. This approach differs from the adaptive mechanism, particularly the fuzzy logics approach, employed in [23].

Substituting (22) into (21) yields

$$\frac{\partial\hat{\boldsymbol{S}}(\boldsymbol{\lambda})}{\partial\boldsymbol{\lambda}^{T}} = -\boldsymbol{K}(\boldsymbol{\Omega}_{ib}^{b}). \tag{23}$$

The solution of (23) can be expressed as the ALC term $\hat{\boldsymbol{S}}(\boldsymbol{\lambda})$ in (12). Substituting $\hat{\boldsymbol{S}}(\boldsymbol{\lambda})$ into (19) and setting $\boldsymbol{D} = \boldsymbol{0}$, the AARNDC term $\hat{\boldsymbol{z}}$ in (13) can be obtained. Then, from (16) and mapping the result to $\mathbb{R}^3$, the gyro bias estimation $\Delta\hat{\boldsymbol{\omega}}_{ib}^{b}$ can be obtained. □

Theorem 2: Subject to the conditions of Theorem 1, if any initial estimation error of gyro bias quaternion vector $\boldsymbol{\Xi}(t_0)$ exists, (12)–(14) ensure that the estimation error of gyro bias quaternion vector $\boldsymbol{\Xi}$ converges asymptotically to zero, that is, $\lim_{t\to\infty}\boldsymbol{\Xi} = \boldsymbol{0}$.

Proof: Since the first component of $\boldsymbol{\Xi}$ is constantly equal to 0, the stability of the observer is only related to the other components of $\boldsymbol{\Xi}$.

Define the positive definite Lyapunov function as

$$V_{\Delta} = \frac{1}{2}\boldsymbol{\Xi}^{T}\boldsymbol{\Xi} > 0. \tag{24}$$

Substituting (17) into the time derivative of (24), we have

$$\dot{V}_{\Delta} = -\boldsymbol{\Xi}^{T}\boldsymbol{L}(\boldsymbol{\lambda}, \boldsymbol{\Omega}_{ib}^{b})\boldsymbol{\Xi}. \tag{25}$$

There exists $\xi_{\min}(\boldsymbol{L}) > 0$, where $\xi_{\min}(\boldsymbol{L})$ is the smallest eigenvalue of matrix $\boldsymbol{L}(\boldsymbol{\lambda}, \boldsymbol{\Omega}_{ib}^{b})$, such that

$$\dot{V}_{\Delta} < -3\xi_{\min}(\boldsymbol{L})\,\|\boldsymbol{\Xi}\|_2^2 < 0 \tag{26}$$

where $\|\bullet\|_2$ signifies the 2-norm of a vector.

This means that $\lim_{t\to\infty}\boldsymbol{\Xi} = \boldsymbol{0}$ if all eigenvalues of $\boldsymbol{L}(\boldsymbol{\lambda}, \boldsymbol{\Omega}_{ib}^{b})$ are positive except 0. □

B. NRBO for Estimating Attitude and Gyro Bias

In this section, we extend the NRBO to incorporate attitude and gyro bias estimation by utilizing both the gyro outputs and the measurements from the noninertial attitude sensor. We propose the NRBO as following, whose scheme is clarified in Fig. 1:

$$\tilde{\boldsymbol{\Lambda}} = \boldsymbol{\Lambda}_o^{-1} \otimes \boldsymbol{\Lambda}_c = 1 \cdot \tilde{\boldsymbol{\Lambda}}_r + \boldsymbol{I}_i^{T} \cdot \tilde{\boldsymbol{\Lambda}}_i, \boldsymbol{e} = 2\tilde{\boldsymbol{\Lambda}}_r\tilde{\boldsymbol{\Lambda}}_i \tag{27}$$

$$\dot{\boldsymbol{\Lambda}}_o = \frac{1}{2}\boldsymbol{\Lambda}_o \otimes H[\boldsymbol{R}_1(\tilde{\boldsymbol{\Lambda}})(\underline{\boldsymbol{\omega}}_{ib}^{b} - \Delta\hat{\boldsymbol{\omega}}_{ib}^{b} + k_a\boldsymbol{e})] \tag{28}$$

$$\hat{\boldsymbol{S}}(\boldsymbol{\lambda}_o) = -\boldsymbol{K}(\boldsymbol{\Omega}_{ib}^{b})\boldsymbol{\lambda}_o \tag{29}$$

$$\dot{\hat{\boldsymbol{z}}} + \boldsymbol{L}(\boldsymbol{\lambda}, \boldsymbol{\Omega}_{ib}^{b})\hat{\boldsymbol{z}} = \boldsymbol{u} \tag{30a}$$

$$\boldsymbol{u} = -\frac{1}{2}\boldsymbol{K}(\boldsymbol{\Omega}_{ib}^{b})\boldsymbol{M}(\boldsymbol{\lambda}_o)\boldsymbol{R}(\tilde{\boldsymbol{\Lambda}})(\underline{\boldsymbol{\Omega}}_{ib}^{b} + k_a\boldsymbol{E}) + \\ + \boldsymbol{L}(\boldsymbol{\lambda}, \boldsymbol{\Omega}_{ib}^{b})\hat{\boldsymbol{S}}(\boldsymbol{\lambda}_o) + k_b\boldsymbol{E} \tag{30b}$$

$$\Delta\hat{\boldsymbol{\omega}}_{ib}^{b} = (h \circ H)^{-1}(\Delta\hat{\boldsymbol{\Omega}}_{ib}^{b}) = (h \circ H)^{-1}[\hat{\boldsymbol{S}}(\boldsymbol{\lambda}_o) - \hat{\boldsymbol{z}}] \tag{31}$$

where $\tilde{\boldsymbol{\Lambda}}$ is a quaternion error, $\tilde{\boldsymbol{\Lambda}}_r \in \mathbb{R}$ is the real part of $\tilde{\boldsymbol{\Lambda}}$, $\tilde{\boldsymbol{\Lambda}}_i \in \mathbb{R}^3$ is the imaginary part of $\tilde{\boldsymbol{\Lambda}}$, $\boldsymbol{R}(\tilde{\boldsymbol{\Lambda}}) = \mathrm{diag}[1, \boldsymbol{R}_1(\tilde{\boldsymbol{\Lambda}})]$, $\boldsymbol{e} \in \mathbb{R}^3$ represents the feedback term, $\boldsymbol{E} = h \circ H(\boldsymbol{e})$, and k_a and k_b are positive gain coefficients. According to (2), when dealing with small attitude errors, $\boldsymbol{e}$ corresponds to the Euler angle error [19]. Prior studies [12], [22] have demonstrated the efficacy of utilizing the real and imaginary components of the quaternion error to construct the feedback term, which proves to be advantageous in estimating attitude and gyro bias.

The proposed NRBO utilizes a deterministic approach, inspired by the Poisson equation. This observer is built upon a

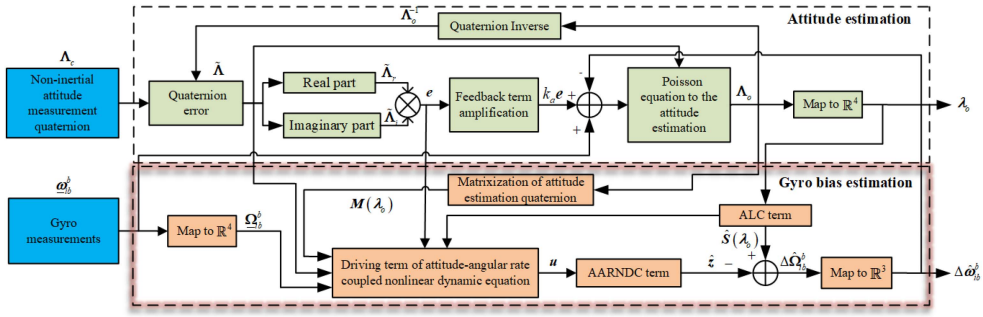

Fig. 1. Scheme of NRBO for estimating attitude and gyro bias.

framework similar to [14] and [19]. However, a notable advantage of the NRBO is its ability to account for the impact of gyro bias resulting from the kinematic states of vehicles during bias estimation. Specifically, the ALC and AARNDC terms are integrated to synthesize the gyro bias estimation, compared with previous approaches that utilize linear feedback of the attitude estimation error. Consequently, this method yields a more precise estimate of the gyro bias. Accurate estimation of gyro bias holds significance due to the higher frequency of the IMU compared with other noninertial attitude sensors within an integrated navigation system. Regular correction of gyro outputs via gyro bias estimation is necessary to provide reliable feedback information for vehicle control systems.

Unlike the deterministic approach, stochastic approach, such as the Kalman filter method, typically rely on the assumption of Gaussian distributions for both measurement and process noise. In contrast, the proposed NRBO does not impose specific assumptions on the noise present in the gyro outputs or the distribution of noninertial attitude sensor measurement noise. Furthermore, this observer offers the advantage of a constant gain setting, leading to a lower computational load compared with the Kalman filter method. The Kalman filter method necessitates recursive linearization of attitude dynamics, matrix inversion, and propagation of a covariance matrix at each computation step for the gain matrix [9]. Undoubtedly, these operations increase the computational load. A comparative analysis conducted in [24] between a nonlinear observer and the multiplicative extended Kalman filter (MEKF) revealed that the computational load of the nonlinear observer is only approximately 20% of the MEKF attitude part.

In subsequent stability analyses, we initially ignore the effect of measurement noise. Doing so is similar to the approach adopted in previous work e.g., [12], [14], [25], [26], and [27], where the stability of nonlinear observers was evaluated without taking into account measurement noise. In Section IV, measurement noise is reintroduced, where the proposed observer performs well in experiments.

Theorem 3: For the nonlinear state equations (10) and (11) under Assumptions 1–3 without consideration of measurement noise, the proposed NRBO (27)–(31) ensures the asymptotic stability of the equilibrium point $[h^T(\tilde{\boldsymbol{\Lambda}}), \boldsymbol{\Xi}^T] = [1, \mathbf{0}^T]$.

Proof: Taking into account (29)–(31), we are able to derive the dynamic equation governing the estimation of the gyro bias quaternion vector $\Delta\hat{\boldsymbol{\Omega}}_{ib}^b$ as

$$\frac{d}{dt}\Delta\hat{\boldsymbol{\Omega}}_{ib}^b = \frac{\partial \hat{\boldsymbol{S}}(\boldsymbol{\lambda}_o)}{\partial \boldsymbol{\lambda}_o^T}\dot{\boldsymbol{\lambda}}_o - \dot{\hat{\boldsymbol{z}}} = \boldsymbol{J}\Delta\hat{\boldsymbol{\Omega}}_{ib}^b - k_b\boldsymbol{E} \tag{32}$$

where

$$\boldsymbol{J} = \frac{1}{2}\boldsymbol{K}(\boldsymbol{\Omega}_{ib}^b)\boldsymbol{M}(\boldsymbol{\lambda}_o)\boldsymbol{R}(\tilde{\boldsymbol{\Lambda}}) - \boldsymbol{L}(\boldsymbol{\lambda}, \boldsymbol{\Omega}_{ib}^b). \tag{33}$$

Hence, by taking into consideration the properties of the gyro bias quaternion vector (11), we can express the variation law of the estimation error of gyro bias quaternion vector $\boldsymbol{\Xi}$

$$\dot{\boldsymbol{\Xi}} = [\boldsymbol{G}(\boldsymbol{\lambda}, \boldsymbol{\Omega}_{ib}^b) - \boldsymbol{J}]\Delta\boldsymbol{\Omega}_{ib}^b + \boldsymbol{J}\boldsymbol{\Xi} + k_b\boldsymbol{E}. \tag{34}$$

Similar to the application of the $\boldsymbol{B} \equiv \mathbf{0}_{4\times4}$ operation discussed in the preceding section (18), in order to ensure that the convergence characteristics of the estimation error $\boldsymbol{\Xi}$ remain unaffected by variations in the gyro bias quaternion vector $\Delta\boldsymbol{\Omega}_{ib}^b$, it becomes imperative to set the coefficient matrix of $\Delta\boldsymbol{\Omega}_{ib}^b$ to zero. Therefore, $\boldsymbol{G}(\boldsymbol{\lambda}, \boldsymbol{\Omega}_{ib}^b)$ is adaptively determined by

$$\boldsymbol{G}(\boldsymbol{\lambda}, \boldsymbol{\Omega}_{ib}^b) + \boldsymbol{L}(\boldsymbol{\lambda}, \boldsymbol{\Omega}_{ib}^b) = \frac{1}{2}\boldsymbol{K}(\boldsymbol{\Omega}_{ib}^b)\boldsymbol{M}(\boldsymbol{\lambda}_o)\boldsymbol{R}(\tilde{\boldsymbol{\Lambda}}). \tag{35}$$

Substituting (35) into (34), we can get

$$\dot{\boldsymbol{\Xi}} = \boldsymbol{J}\boldsymbol{\Xi} + k_b\boldsymbol{E}. \tag{36}$$

The attitude error dynamics equation can be described according to (27) and (28)

$$\dot{\tilde{\boldsymbol{\lambda}}} = \frac{1}{2}\begin{bmatrix} 0 & \tilde{\boldsymbol{\omega}}^T \\ -\tilde{\boldsymbol{\omega}} & \tilde{\boldsymbol{\omega}}^\times \end{bmatrix}\tilde{\boldsymbol{\lambda}} \tag{37}$$

where $\tilde{\boldsymbol{\lambda}} = h(\tilde{\boldsymbol{\Lambda}})$ is quaternion error vector, and $\tilde{\boldsymbol{\omega}} = \boldsymbol{\xi} + k_a\boldsymbol{e}$, $\boldsymbol{\xi} = (h \circ H)^{-1}(\boldsymbol{\Xi})$.

Considering the error dynamics (36) and (37), we select the Lyapunov function as

$$V = 2(1 - \tilde{\boldsymbol{\Lambda}}_r^2) + \frac{1}{2k_b}\|\boldsymbol{\Xi}\|_2^2. \tag{38}$$

where $1 - \tilde{\boldsymbol{\Lambda}}_r^2$ is referred to as the potential function on unit quaternions, and it is directly related to the feedback term $\boldsymbol{e}$ in (27) by $\boldsymbol{e} = -\nabla(1 - \tilde{\boldsymbol{\Lambda}}_r^2)\tilde{\boldsymbol{\Lambda}}_i$ [22]. Moreover, the type of Lyapunov function designed as (38) has been demonstrated to exhibit robustness to noise interference, as evidenced in [28].

Due to the property of the unit quaternion, $\tilde{\mathbf{\Lambda}}_r^2 \leq 1$, so $V > 0$. The relationship between quaternion and DCM [19] is

$$2\left(1-\tilde{\mathbf{\Lambda}}_r^2\right) = \frac{1}{2}\mathrm{tr}(\boldsymbol{I}_3 - \tilde{\boldsymbol{R}}_1) \tag{39}$$

where $\tilde{\boldsymbol{R}}_1 = \hat{\boldsymbol{R}}_1^T \boldsymbol{R}_1 = \boldsymbol{I}_3 + \boldsymbol{e}^\times$, $\boldsymbol{e}^\times = \frac{1}{2}(\tilde{\boldsymbol{R}}_1 - \tilde{\boldsymbol{R}}_1^T)$, and $\mathrm{tr}(\bullet)$ signifies the trace of a matrix. Therefore, the equivalent form of (38) can be rewritten as follows:

$$V = \frac{1}{2}\mathrm{tr}(\boldsymbol{I}_3 - \tilde{\boldsymbol{R}}_1) + \frac{1}{2k_b}\left\|\boldsymbol{\Xi}\right\|_2^2. \tag{40}$$

Then, from [12] and [19] and considering (7), we get the time derivative of (40)

$$\begin{aligned}
\dot{V} = & -\frac{1}{2}\mathrm{tr}\left(\dot{\tilde{\boldsymbol{R}}}_1\right) + \frac{1}{k_b}\boldsymbol{\Xi}^T\dot{\boldsymbol{\Xi}} \\
= & -\frac{1}{2}\mathrm{tr}\left[\left(k_a\boldsymbol{e}+\boldsymbol{\xi}\right)^\times \tilde{\boldsymbol{R}}_1\right] + \frac{1}{k_b}\boldsymbol{\Xi}^T\dot{\boldsymbol{\Xi}} \\
= & -\frac{k_a}{2}\mathrm{tr}\left\{\boldsymbol{e}^\times\left[\frac{1}{2}\left(\tilde{\boldsymbol{R}}_1+\tilde{\boldsymbol{R}}_1^T\right)+\frac{1}{2}\left(\tilde{\boldsymbol{R}}_1-\tilde{\boldsymbol{R}}_1^T\right)\right]\right\} \\
& -\frac{1}{2}\mathrm{tr}\left\{\boldsymbol{\xi}^\times\left[\frac{1}{2}\left(\tilde{\boldsymbol{R}}_1+\tilde{\boldsymbol{R}}_1^T\right)+\frac{1}{2}\left(\tilde{\boldsymbol{R}}_1-\tilde{\boldsymbol{R}}_1^T\right)\right]\right\} \\
& +\frac{1}{k_b}\boldsymbol{\Xi}^T\dot{\boldsymbol{\Xi}} \\
= & -\frac{k_a}{2}\mathrm{tr}\left[\left(\boldsymbol{e}^\times\right)^2\right] - \frac{1}{2}tr\left(\boldsymbol{\xi}^\times\boldsymbol{e}^\times\right) + \frac{1}{k_b}\boldsymbol{\Xi}^T\dot{\boldsymbol{\Xi}} \\
= & -k_a\left\|\boldsymbol{e}\right\|_2^2 - \boldsymbol{\xi}^T\boldsymbol{e} + \boldsymbol{\Xi}^T\boldsymbol{E} + \frac{1}{k_b}\boldsymbol{\Xi}^T\boldsymbol{J}\boldsymbol{\Xi} \\
= & -k_a\left\|\boldsymbol{e}\right\|_2^2 + \frac{1}{k_b}\boldsymbol{\Xi}^T\left(\frac{1}{2}\boldsymbol{K}\boldsymbol{M}\boldsymbol{R} - \boldsymbol{L}\right)\boldsymbol{\Xi} \\
< & -k_a\left\|\boldsymbol{e}\right\|_2^2 - \frac{1}{2k_b}(2l-k)\left\|\boldsymbol{\xi}\right\|_2^2 < 0
\end{aligned} \tag{41}$$

where $k = \xi_{\max}[\boldsymbol{K}(\boldsymbol{\Omega}_{ib}^b)] < \sigma_{\min}[\boldsymbol{M}(\boldsymbol{\lambda}_o)\boldsymbol{R}(\tilde{\boldsymbol{\Lambda}})]$, here $\sigma_{\min}$ denotes the minimum singular value. From (2) and (6), and since $\boldsymbol{M}$ and $\boldsymbol{R}$ are orthogonal matrices, the singular values of their product are eigenvalues of $\sqrt{(\boldsymbol{M}\boldsymbol{R})^T(\boldsymbol{M}\boldsymbol{R})} = \boldsymbol{I}_4$, i.e., $k < 1$, and $l = \xi_{\min}[\boldsymbol{L}(\boldsymbol{\lambda}, \boldsymbol{\Omega}_{ib}^b)] > \frac{1}{2}k$. This design of the gains ensures that $V > 0$ and $\dot{V} < 0$, simultaneously. □

Based on the unit quaternion property, the elements of matrix $\boldsymbol{M}(\boldsymbol{\lambda}_o)$ have absolute values less than or equal to 1. As the attitude error approaches zero, the matrix $\boldsymbol{R}(\tilde{\boldsymbol{\Lambda}})$ converges to the identity matrix. Through stability analysis, it is recommended to design the elements in matrix $\boldsymbol{K}(\boldsymbol{\Omega}_{ib}^b)$ to be small within the stable range. Conversely, the elements in matrix $\boldsymbol{L}(\boldsymbol{\lambda}, \boldsymbol{\Omega}_{ib}^b)$ should be designed to be large within the stable range to allow the dominant diagonal elements in matrix $\boldsymbol{L}(\boldsymbol{\lambda}, \boldsymbol{\Omega}_{ib}^b)$ to ensure that $\boldsymbol{J}$ is negative definite. So, (36) can be approximated in $\mathbb{R}^3$ as

$$\dot{\boldsymbol{\xi}} + \boldsymbol{L}_1(\boldsymbol{\lambda}, \boldsymbol{\Omega}_{ib}^b)\boldsymbol{\xi} = k_b\boldsymbol{e} \tag{42}$$

where $\boldsymbol{L}(\boldsymbol{\lambda}, \boldsymbol{\Omega}_{ib}^b) = \mathrm{diag}[0, \boldsymbol{L}_1(\boldsymbol{\lambda}, \boldsymbol{\Omega}_{ib}^b)]$.

According to (42), performance metrics for the estimation error of gyro bias vector $\boldsymbol{\xi}$ can be written as

$$I = \int_0^\infty f(\boldsymbol{\xi}, \dot{\boldsymbol{\xi}})\,dt = \int_0^\infty (\boldsymbol{\chi}\boldsymbol{T}\boldsymbol{\chi}^T)dt \tag{43}$$

where

$$\boldsymbol{\chi} = \begin{bmatrix}\boldsymbol{\xi}^T & \dot{\boldsymbol{\xi}}^T & \boldsymbol{e}^T\end{bmatrix}, \boldsymbol{T} = \begin{bmatrix}-\boldsymbol{I}_3 & \boldsymbol{0} & k_b\boldsymbol{I}_3 \\ \boldsymbol{0} & -\boldsymbol{L}_1^2 & k_b\boldsymbol{L}_1 \\ k_b\boldsymbol{I}_3 & k_b\boldsymbol{L}_1 & \boldsymbol{0}\end{bmatrix}. \tag{44}$$

Note that

$$\det(\boldsymbol{T}) = 2k_b^2\det(\boldsymbol{L}_1^2) > 0$$

which means that the integrand of the performance metrics is positive definite. The Euler–Lagrange equation can be employed to determine the extrema of the functional (43)

$$\begin{aligned}
\frac{d}{dt}\left(\frac{\partial f}{\partial \dot{\boldsymbol{\xi}}^T}\right) - \frac{\partial f}{\partial \boldsymbol{\xi}^T} = -2\frac{d}{dt}(\dot{\boldsymbol{\xi}} + \boldsymbol{L}_1\boldsymbol{\xi} - k_b\boldsymbol{e}) \\
+ 2\boldsymbol{L}_1(\dot{\boldsymbol{\xi}} + \boldsymbol{L}_1\boldsymbol{\xi} - k_b\boldsymbol{e}) = \boldsymbol{0}.
\end{aligned} \tag{45}$$

Therefore, (42) corresponds to a solution of (45). Consequently, the gyro bias estimated through NRBO ensures that the estimation error complies with the performance metrics outlined in (43) and (44).

Given the specified performance metrics, accurately assessing gyro bias estimation becomes crucial, especially when the true value of gyro bias is not accessible in practical applications. To address this, a method known as bias-corrected gyro integrating (BCGI) is employed, which has been widely used in recent years to gauge the quality of gyro bias estimation [29], [30]. BCGI involves correcting the gyro outputs with the estimated gyro bias to drive the Poisson equation

$$\dot{\boldsymbol{\Lambda}}_{\mathrm{BCGI}} = \frac{1}{2}\boldsymbol{\Lambda}_{\mathrm{BCGI}} \otimes H(\underline{\boldsymbol{\omega}}_{ib}^b - \Delta\hat{\boldsymbol{\omega}}_{ib}^b). \tag{46}$$

From (46), it can be observed that if the estimated gyro bias is accurate, meaning $\Delta\hat{\boldsymbol{\omega}}_{ib}^b \to \Delta\boldsymbol{\omega}_{ib}^b$, then $\boldsymbol{\Lambda}_{\mathrm{BCGI}}$ tends to converge toward the reference attitude.

According to Theorem 3, without taking measurement noise into account, the designed observer guarantees convergence of the attitude estimation error $\boldsymbol{e} \to \boldsymbol{0}$ and gyro estimation error $\boldsymbol{\xi} \to \boldsymbol{0}$. To prevent over-idealization of the designed observer, it becomes imperative to account for the influence of measurement noise. In recent years, the consideration of measurement noise in deterministic observers has gained prominence. For instance, Tong et al. [12] extended their analysis to include the input-to-state stability of the observer, where measurement noise serves as input. The upper bounds on measurement noise levels that ensure observer stability have been explored by the authors in [22] and [31]. In these studies, a comparison has been made between the behavior of the Lyapunov function and its derivatives in the presence and absence of measurement noise. Inspired by these studies, we reconsider Assumption 2 by introducing measurement noise $\Delta\boldsymbol{\Psi}$ into the system. Subsequently, with the

presence of measurement noise $\Delta\boldsymbol{\Psi}$, we employ the results from Theorem 3 to reassess the stability analysis.

Theorem 4: Consider the designed observer (27)–(31) under Assumption 2 with the presence of measurement noise $\Delta\boldsymbol{\Psi}$. Define a closed neighborhood $\mathcal{M}$ of $\{\boldsymbol{e}=0,\boldsymbol{\xi}=0\}$

$$\mathcal{M}:=\{(\boldsymbol{e},\boldsymbol{\xi}):\|\boldsymbol{e}\|_2\leq c_4,\|\boldsymbol{\xi}\|_2\leq c_5\} \tag{47}$$

where $c_4,c_5>0$. If the 2-norm of the measurement noise $\Delta\boldsymbol{\Psi}$ satisfies the following inequality:

$$\|\Delta\boldsymbol{\Psi}\|_2\leq\eta<c_4+\frac{2l-k}{2k_ak_b}\frac{c_5^2}{c_4} \tag{48}$$

then, both the attitude estimation error $\boldsymbol{e}$ and the gyro bias estimation error $\boldsymbol{\xi}$ converge to the closed neighborhood $\mathcal{M}$.

Proof: The attitude error dynamics can be expressed by the DCM with consideration of measurement noise $\Delta\boldsymbol{\Psi}$ as follows [22], [31]:

$$\dot{\tilde{\boldsymbol{R}}}_1=(k_a\boldsymbol{e}+\boldsymbol{\xi}+k_a\Delta\boldsymbol{\Psi})^{\times}\tilde{\boldsymbol{R}}_1. \tag{49}$$

Using the Lyapunov function (40) in the proof of Theorem 3, we recalculate its derivative with consideration of (49)

$$\begin{aligned}\dot{V}=&-\frac{1}{2}tr\left[(k_a\boldsymbol{e}+\boldsymbol{\xi}+k_a\Delta\boldsymbol{\Psi})^{\times}\tilde{\boldsymbol{R}}_1\right]+\frac{1}{k_b}\boldsymbol{\Xi}^T\dot{\boldsymbol{\Xi}}\\<&-k_a\|\boldsymbol{e}\|_2^2-\frac{1}{2k_b}(2l-k)\|\boldsymbol{\xi}\|_2^2-k_a\boldsymbol{e}^T\Delta\boldsymbol{\Psi}.\end{aligned} \tag{50}$$

It is noteworthy, as indicated by (50), that the derivative of the Lyapunov function incorporates an additional term arising from the presence of measurement noise. This differs from (41), which does not take measurement noise into consideration, for the derivative of $\dot{V}$. Using Cauchy–Schwarz inequality with the upper bounds in (47) and (48), we deduce that

$$-\boldsymbol{e}^T\Delta\boldsymbol{\Psi}\leq\|\boldsymbol{e}\|_2\|\Delta\boldsymbol{\Psi}\|_2\leq c_4\eta. \tag{51}$$

Therefore, the upper bound of $\dot{V}$ is

$$\dot{V}<-k_a\|\boldsymbol{e}\|_2^2-\frac{1}{2k_b}(2l-k)\|\boldsymbol{\xi}\|_2^2+k_ac_4\eta. \tag{52}$$

Along the boundary of the neighborhood $\mathcal{M}$ defined by (47), the upper bound on $\dot{V}$ is characterized by

$$\dot{V}<-k_ac_4^2-\frac{1}{2k_b}(2l-k)c_5^2+k_ac_4\eta. \tag{53}$$

$\dot{V}$ exhibits a negative value along the boundary of $\mathcal{M}$ when

$$-k_ac_4^2-\frac{1}{2k_b}(2l-k)c_5^2+k_ac_4\eta<0 \tag{54}$$

which is a sufficient condition for all trajectories starting outside the neighborhood of $\{\boldsymbol{e}=0,\boldsymbol{\xi}=0\}$ to converge to $\mathcal{M}$. Alternatively, (54) yields the following equation for the ratio of observer gains:

$$\frac{2k_ak_b}{2l-k}<\frac{c_5^2}{c_4\eta-c_4^2}. \tag{55}$$

This establishes a connection between the ratio of $\frac{2k_ak_b}{2l-k}$ and the upper bound on the 2-norm of the measurement noise $\Delta\boldsymbol{\Psi}$, as well as the boundaries of the neighborhood $\mathcal{M}$. This relationship ensures the convergence of the attitude estimation error $\boldsymbol{e}$ and the gyro estimation error $\boldsymbol{\xi}$ to the neighborhood of $\{\boldsymbol{e}=0,\boldsymbol{\xi}=0\}$. □

In order to enhance the effectiveness of the proposed observer, a parameter-tuning strategy becomes necessary. Several factors must be taken into consideration, including convergence speed, noise level, and gyro bias characteristics. The analysis of the Lyapunov function derivative in (50) sheds light on the significance of selecting a suitable positive gain k_a. On the one hand, the term $-k_a\|\boldsymbol{e}\|_2^2$ demonstrates that increasing the value of k_a accelerates the system's convergence rate. However, on the other hand, it is important to note that a higher k_a also amplifies the impact of measurement noise, as evidenced by $k_a\Delta\boldsymbol{\Psi}$ in (49). Therefore, it is crucial to strike a balance while choosing k_a. As demonstrated in (28), $k_a\boldsymbol{e}$ serves as a feedback term to compensate for gyro outputs $\underline{\boldsymbol{\omega}}_{ib}^b$. In the presence of measurement noise, both $k_a\Delta\boldsymbol{\Psi}$ and $k_a\boldsymbol{e}$ appear together, as shown in (49). Therefore, the parameter k_a should be chosen judiciously to ensure that the noise level of $k_a\Delta\boldsymbol{\Psi}$ remains lower than the noise level in gyro outputs $\underline{\boldsymbol{\omega}}_{ib}^b$. This choice of k_a is feasible and practical in real-world applications. In (32), the feedback quaternion vector $\boldsymbol{E}$ is amplified by k_b, and the estimation of the gyro bias quaternion vector is acquired through integral action. Under Assumption 3, which assumes the boundedness of the gyro bias, the value of k_b should not be excessively large to avoid over-amplification of the feedback quaternion vector $\boldsymbol{E}$, which could introduce oscillations in the estimation of the gyro bias. As demonstrated in (55), it becomes evident that a relatively modest value for k_b is more likely to fulfill the inequality. Considering the slow variations of the gyro bias, indicating the presence of the bias instability, the eigenvalue of $\boldsymbol{G}(\boldsymbol{\lambda},\boldsymbol{\Omega}_{ib}^b)$ in (11) becomes relatively small. This characteristic can be identified through the Allan variance analysis technique [32]. Consequently, the eigenvalues of the diagonal matrix $\boldsymbol{L}(\boldsymbol{\lambda},\boldsymbol{\Omega}_{ib}^b)$ in (35) are of a similar magnitude. According to stability analysis (41), the magnitude of the eigenvalues of matrix $\boldsymbol{K}(\boldsymbol{\Omega}_{ib}^b)$ should be smaller than the magnitude of the eigenvalues of matrix $\boldsymbol{L}(\boldsymbol{\lambda},\boldsymbol{\Omega}_{ib}^b)$.

IV. Experiment Results

To validate the performance of the proposed NRBO, we considered the case of an end-effector of cable-driven parallel robot vibration as a test bed.

The thorny aspect of the experiment is the vibration caused by the under-constrained end-effector. This leads to rapidly changing attitudes and angular velocities, which negatively affect the operating environment of the MEMS gyros. The experimental platform is depicted in Fig. 2(a).

The platform includes four ESTUN servo motors positioned at the apex of a 4.8 m × 3.8 m rectangle with a height of 2.5 m from the ground. Between each adjacent motor, two Flex 13 motion capture cameras are installed, offering capture rates ranging from 30 to 200 Hz. The Optitrack system is composed of these eight motion capture cameras. To connect the motors with the end-effector, flexible cables are used. The end-effector, illustrated in Fig. 2(b), accommodates the WCG-1 IMU sensor

(a) (b)

Fig. 2. (a) Cable-driven parallel robot experimental platform. (b) End-effector.

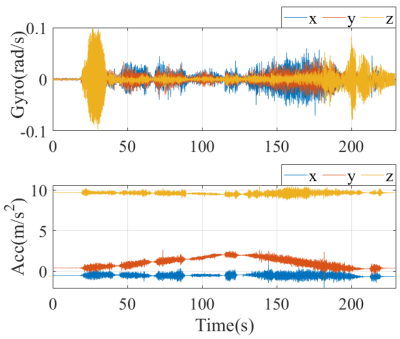

Fig. 3. Outputs of WCG-1 IMU in the dynamic experiment of the cable-driven parallel robot.

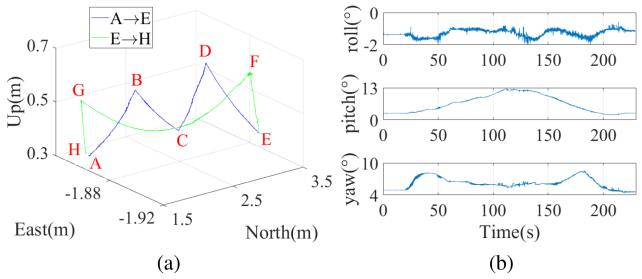

(a) (b)

Fig. 4. End-effector trajectory after processing of (a) End-effector trajectory after processing of Motive software. (b) The raw attitudes of end-effector output by Optitrack system.

within an antistatic safety enclosure. The IMU data is logged at a 200 Hz sampling rate, with a gyro bias stability of approximately $15^\circ/\text{h}$. The angular velocities and accelerations output by the WCG-1 IMU are shown in Fig. 3. The central processing unit inside the end-effector consists of the STM32F030K6T6 microcontroller and Raspberry 4B embedded computer. To enhance data transmission speed, stability, and security, wireless LAN and TCP/IP protocols are employed to connect with the motor drive system and communicate with the end-effector.

The noninertial sensor measurements utilized here are the raw attitudes obtained from the Optitrack system, as shown in Fig. 4(b). These raw attitudes are fused with the angular velocities output from the IMU to estimate both attitude and gyro bias. To obtain the reference attitudes, the Motive software is employed to process the raw attitudes obtained from the Optitrack system. It is worth noting that the raw attitudes are sensitive to light conditions [33] and have nonequal intervals. The accuracy of the reference attitudes is less than 0.005° after processing [34]. By comparing the raw attitudes with the reference, it is possible to calculate a noise variance of $(0.06^\circ)^2$ for the raw attitudes.

In this experiment, a flexible cable controlled by motors allows the end-effector of the cable-driven parallel robot to follow a specific trajectory [see Fig. 4(a)] within the workspace. The end-effector motion lasted 229.16 s. The end-effector is at rest for the first 18 s at point A. From 18 to 115 s, it completes the trajectory from point A to point E, passing through three turning points B, C, and D. From 115 to 220 s, the end-effector moves from point E to point H and stays for 9 s to end the experiment. The end-effector reaches points B–G at 42, 67, 90, 115, 124, and 206, respectively, with a stopping time of 2 to 3 s each.

Considering that the frequency of Optitrack output attitudes is different from the IMU output frequency, an asynchronous sensor fusion strategy is adopted. Four attitude estimation algorithms are evaluated, including GI, NNO [14], IEKF [13], and the proposed NRBO.

Guided by Allan variance analysis and considering the noise level of the noninertial sensor measurements, the parameters of NRBO are designed based on the principles described in Section III as $k_a = 3$ rad/s, $k_b = 0.5$ rad/s, $\boldsymbol{L} = \text{diag}(0, 1.3 \times 10^{-4}, 6.5 \times 10^{-5}, 1.1 \times 10^{-4})\text{s}^{-1}$, and $\boldsymbol{K} = 0.2\boldsymbol{L}$. The tuning parameters in NNO are designed as $k_1 = 3.5$, $k_2 = 0.07$, $\rho_1 = 1$, and $\rho_2 = 1$. In IEKF, the initial conditions for the estimated states are set as $\boldsymbol{x}_{0|0} = \boldsymbol{0}_{6\times1}$ and $\boldsymbol{P}_{0|0} = \text{diag}(10^{-3}\text{rad}\boldsymbol{I}_{3\times1}, 10^{-3}\text{rad/s}\boldsymbol{I}_{3\times1})^2$, the state noise covariance matrix $\boldsymbol{Q}_k$ is set as $\text{diag}(10^{-5}\text{rad}\boldsymbol{I}_{3\times1}, 10^{-6}\text{rad/s}\boldsymbol{I}_{3\times1})^2$ and the measurement noise covariance matrix $\boldsymbol{R}_k$ is set as $\text{diag}(10^{-3}\text{rad}\boldsymbol{I}_{3\times1})^2$. The estimated attitudes with reference attitudes and attitude estimation errors are illustrated in Fig. 5. The gyro biases estimated by NNO, IEKF, and NRBO are shown in Fig. 6.

Note from Fig. 5 that the GI estimated attitudes deviate from the reference attitudes in less than 20 s. This is due to the accumulation of the gyro biases. In contrast, the RMS of estimation errors for attitude in NNO, IEKF, and NRBO algorithms do not exceed 0.2°, which is due to the participation of the attitude information of the end-effector output by the Optitrack system in the attitude estimation and the accurate attitude kinematic model. It is verified that the attitude estimation accuracy can be guaranteed with a direct observable and accurate model.

From Fig. 6, NNO, IEKF, and NRBO provide the estimated gyro biases. The gyro biases estimated by NNO change slowly, and the gyro biases estimated by IEKF oscillate around zero. While the gyro biases estimated by NRBO converge rapidly to 3.5×10^{-3} rad/s, 1×10^{-3} rad/s, and 5.7×10^{-3} rad/s, respectively. After convergence, the estimated gyro drifts are given by NRBO near the estimated gyro biases.

We evaluate the gyro bias estimation accuracy utilizing BCGI (46) after correcting gyro outputs with the estimated gyro biases obtained from NNO, IEKF, and NRBO, respectively. The results are depicted in Fig. 7, denoted as BCGI _ NNO, BCGI _ IEKF, and BCGI _ NRBO, respectively. The RMS of estimation errors for attitudes before correction of gyro outputs in GI, and after correction of gyro outputs with gyro bias estimation in

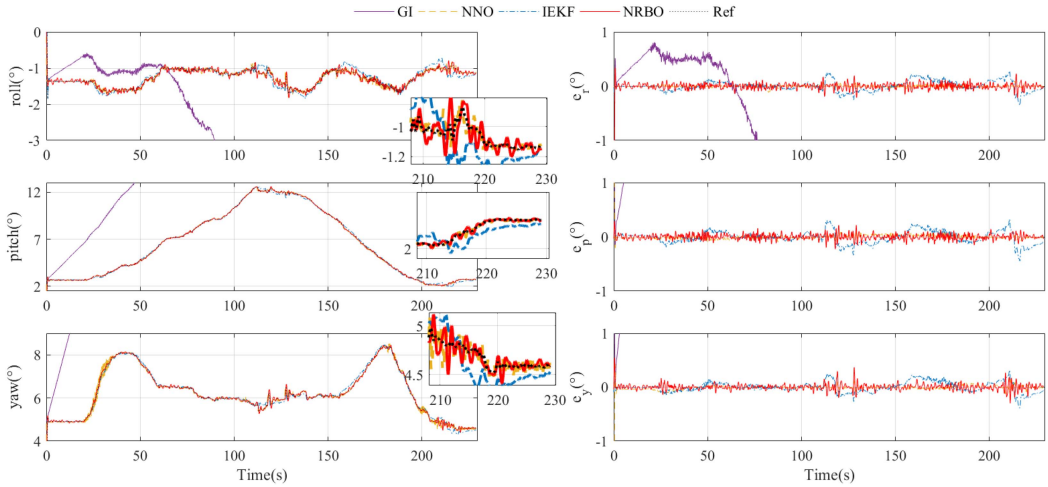

Fig. 5. End-effector attitude estimation by different algorithms under vibration.

TABLE I
RMS OF ESTIMATION ERRORS FOR ATTITUDES BEFORE AND AFTER CORRECTION OF GYRO OUTPUTS WITH GYRO BIAS ESTIMATION

	Roll (°)	Pitch (°)	Yaw (°)
Before correction			
GI	11.18	21.02	48.53
After correction			
BCGI_NNO	0.80	3.56	11.05
BCGI_IEKF	10.68	19.75	47.31
BCGI_NRBO	0.078	0.107	0.153

BCGI _ NNO, BCGI _ IEKF, and BCGI _ NRBO are presented in Table I.

From Fig. 7, it can be observed that the steady-state errors of the roll in BCGI _ NNO are maintained within 3° after 120 s, while the pitch in BCGI _ NNO results in overcompensation. The limitations of accuracy improvement in yaw become apparent in BCGI _ NNO. This indicates that although NNO partially estimates the gyro biases, the estimates are not accurate simultaneously in all three axes. As for BCGI _ IEKF, both pitch and yaw deviate from the reference attitude by more than 10°. This indicates that although IEKF estimates gyro biases, they fail to converge by the end of the experiment. On the other hand, BCGI _ NRBO estimated attitude approaches the reference one, with RMS estimation errors for attitudes not exceeding 0.2°, indicating that the NRBO estimates gyro biases with high accuracy. This result demonstrates that the assumption of NRBO about the nonlinearity of gyro bias effectively recovers the uncertainties and nonlinearities associated with the gyro bias itself. The assumption of the nonlinear model of gyro bias in this article is verified, and the advantage of the NRBO algorithm in the case of an unknown gyro drift model is demonstrated.

In order to examine the robustness of the NRBO with a deterministic approach to measurement noise, different levels of white noise are introduced to contaminate the noninertial sensor measurements. As comparisons, NNO and IEKF are considered. Notably, the parameters of the NNO, IEKF, and NRBO remain unchanged throughout the analysis. The RMS of

TABLE II
RMS OF ESTIMATION ERRORS FOR ATTITUDES WITH AUGMENTED MEASUREMENT NOISE

Method	Total noise level of $\Delta\Psi_i, i = \mathrm{R, P, Y}$	Roll (°)	Pitch (°)	Yaw (°)
NNO	$(0.12°)^2$	0.067	0.087	0.118
	$(0.24°)^2$	0.072	0.091	0.122
	$(0.36°)^2$	0.081	0.098	0.130
IEKF	$(0.12°)^2$	0.087	0.103	0.115
	$(0.24°)^2$	0.091	0.118	0.127
	$(0.36°)^2$	0.098	0.137	0.152
NRBO	$(0.12°)^2$	0.065	0.078	0.117
	$(0.24°)^2$	0.070	0.082	0.120
	$(0.36°)^2$	0.075	0.089	0.124

TABLE III
RMS OF BCGI ESTIMATED ATTITUDE ERRORS WITH AUGMENTED MEASUREMENT NOISE

Method	Total noise level of $\Delta\Psi_i, i = \mathrm{R, P, Y}$	Roll (°)	Pitch (°)	Yaw (°)
BCGI_NNO	$(0.12°)^2$	0.083	3.57	11.06
	$(0.24°)^2$	0.113	3.59	11.08
	$(0.36°)^2$	0.180	3.65	11.15
BCGI_IEKF	$(0.12°)^2$	10.78	20.01	47.48
	$(0.24°)^2$	10.80	20.05	47.50
	$(0.36°)^2$	10.92	20.16	47.62
BCGI_NRBO	$(0.12°)^2$	0.089	0.114	0.162
	$(0.24°)^2$	0.122	0.155	0.189
	$(0.36°)^2$	0.130	0.175	0.235

estimation errors for attitude in NRBO, as well as in NNO and IEKF is displayed in Table II. Based on the outcomes presented in Table II, as the levels of measurement noise increased from 100% to 500%, the RMS norm of estimation errors for attitudes $\|\boldsymbol{e}\|_{\mathrm{RMS}}$ in NNO, IEKF, and NRBO increased by 0.037°, 0.082°, and 0.028°, respectively. Furthermore, to evaluate the gyro bias estimations accomplished by the NRBO in the presence of augmented measurement noise, the estimated gyro biases are utilized to correct the gyro outputs, subsequently obtaining the BCGI _ NRBO estimated attitudes via (46). For comparative purposes, BCGI _ NNO and BCGI _ IEKF are also considered.

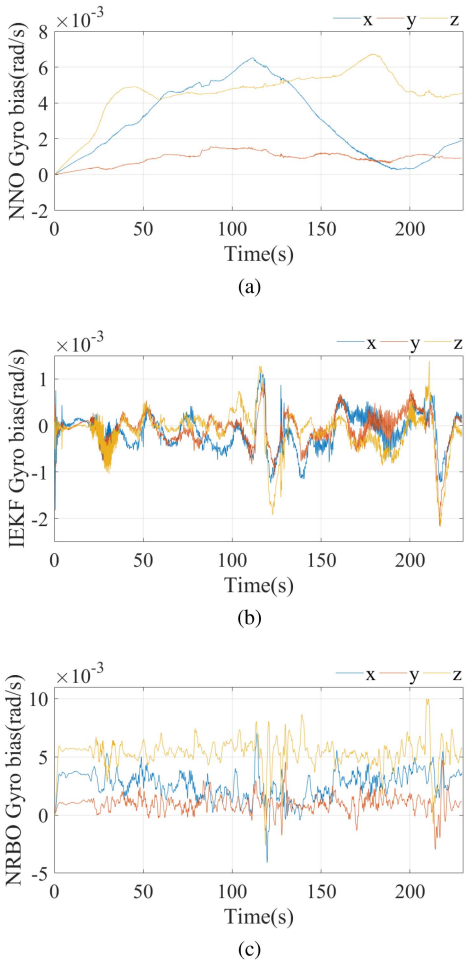

Fig. 6. Estimation results. Gyro bias estimation by (a) NNO, (b) IEKF, and (c) NRBO under vibration.

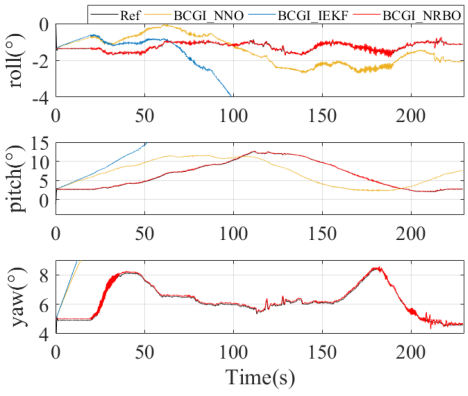

Fig. 7. End-effector attitude estimation by BCGI.

The RMS of BCGI _ NNO, BCGI _ IEKF, and BCGI _ NRBO estimated attitude errors with augmented measurement noise are presented in Table III. As indicated by the results in Table III, with an escalation in measurement noise levels from 100% to 500%, the RMS norm of BCGI _ NNO, BCGI _ IEKF, and BCGI _ NRBO estimated attitude errors increased by 0.267°, 0.430°, and 0.175°, respectively. These findings underscore the robustness of the robustness of NRBO to noise, despite its deterministic approach.

V. Conclusion

In this article, we proposed an NRBO with online observation for the commercial-grade MEMS gyros bias using gyro outputs and noninertial attitude measurements. The primary difference between the proposed algorithm and the traditional ones is that it takes into account the nonlinear characteristics of MEMS gyro bias, i.e., the gyro bias is no longer considered as constant. We developed a dynamics-sensitive gyro bias estimation method and demonstrated the stability of NRBO, ensuring convergence of attitude and gyro bias estimation errors simultaneously. In addition, we provided specified performance metrics for gyro bias estimation error.

In the dynamic experiment of the cable-driven parallel robot, the gyro biases were estimated by NRBO in the case of the end-effector wobbling caused by the elasticity of the flexible cable and unknown initial gyro bias. To validate the accuracy of gyro bias estimation by NRBO, we employed the BCGI method. The attitudes after the correction of gyro outputs with gyro bias estimation by NRBO have been shown in Fig. 7, and the RMS of the estimation errors, listed in Table I. The results of the above experiment indicated that the nonlinear features in the gyro bias estimated by NRBO were restored as much as possible, which improved the estimation accuracy. In addition, we investigated the robustness of the NRBO against measurement noise by introducing additional noise, and the results are presented in Tables II and III.

Future efforts will focus on analyzing the observability of the NRBO proposed in this article, which will be extended to bias estimation for other motion sensors.

References

[1] S. Koenig et al., "Towards a navigation grade si-mems gyroscope," in *Proc. DGON Inertial Sensors Syst.*, 2019, pp. 1–18.

[2] R. Bhardwaj, N. Kumar, and V. Kumar, "Errors in micro-electro-mechanical systems inertial measurement and a review on present practices of error modelling," *Trans. Inst. Meas. Control*, vol. 40, no. 9, pp. 2843–2854, 2018.

[3] A. Nazemipour, M. T. Manzuri, D. Kamran, and M. Karimian, "MEMS gyro bias estimation in accelerated motions using sensor fusion of camera and angular-rate gyroscope," *IEEE Trans. Veh. Technol.*, vol. 69, no. 4, pp. 3841–3851, Apr. 2020.

[4] Z. Qiu, J. Yang, and L. Guo, "Stochastic stable attitude estimation algorithm using UKF with measurement loss," *IEEE/ASME Trans. Mechatron.*, vol. 27, no. 2, pp. 1059–1069, Apr. 2022.

[5] W. Ding and Y. Gao, "Attitude estimation using low-cost MARG sensors with disturbances reduction," *IEEE Trans. Instrum. Meas.*, vol. 70, Aug. 12, 2021, Art. no. 1009111.

[6] A. D. Kahn and D. J. Edwards, "Navigation, guidance, and control of a micro unmanned aerial glider," *J. Guid., Control, Dyn.*, vol. 42, no. 11, pp. 2474–2484, 2019.

[7] X. Shen, D. Yuan, R. Chang, and W. Jin, "A nonlinear observer for attitude estimation of vehicle-mounted Satcom-on-the-Move," *IEEE Sensors J.*, vol. 19, no. 18, pp. 8057–8066, Sep. 2019.

[8] M. Lungu, "Control of double gimbal control moment gyro systems using the backstepping control method and a nonlinear disturbance observer," *Acta Astronautica*, vol. 180, pp. 639–649, 2021.

[9] J. Keighobadi, M. Hosseini-Pishrobat, J. Faraji, and M. N. Langehbiz, "Design and experimental evaluation of immersion and invariance observer for low-cost attitude-heading reference system," *IEEE Trans. Ind. Electron.*, vol. 67, no. 9, pp. 7871–7878, Sep. 2020.

[10] J. Reis, P. Batista, P. Oliveira, and C. Silvestre, "Earth velocity and rigid-body attitude estimation on SO(3) using biased measurements," *IEEE/ASME Trans. Mechatron.*, vol. 27, no. 6, pp. 4246–4257, Dec. 2022.
[11] E. Bjørne, E. F. Brekke, T. H. Bryne, and T. A. Johansen, "Semiglobally asymptotically stable nonlinear observer for camera aided navigation," *IEEE Trans. Control Syst. Technol.*, vol. 29, no. 5, pp. 2279–2286, Sep. 2021.
[12] X. Tong, M. Chen, and F. Yang, "Robust hybrid attitude and gyro-bias observer on quaternions," *IEEE Trans. Ind. Electron.*, vol. 69, no. 8, pp. 8545–8553, Aug. 2022.
[13] A. Barrau and S. Bonnabel, "The invariant extended Kalman filter as a stable observer," *IEEE Trans. Autom. Control*, vol. 62, no. 4, pp. 1797–1812, Apr. 2017.
[14] S. Berkane, A. Tayebi, and S. De Marco, "A nonlinear navigation observer using IMU and generic position information," *Automatica*, vol. 127, 2021, Art. no. 109513.
[15] L. Fusini, T. I. Fossen, and T. A. Johansen, "Nonlinear observers for GNSS- and camera-aided inertial navigation of a fixed-wing UAV," *IEEE Trans. Control Syst. Technol.*, vol. 26, no. 5, pp. 1884–1891, Sep. 2018.
[16] Y. Wang, R. Cao, C. Li, and R. N. Dean, "Concepts, roadmaps and challenges of ovenized MEMS gyroscopes: A review," *IEEE Sensors J.*, vol. 21, no. 1, pp. 92–119, Jan. 2021.
[17] V. I. Finaev, M. Y. Medvedev, V. K. Pshikhopov, V. A. Pereverzev, and V. V. Soloviev, "Unmanned powerboat motion terminal control in an environment with moving obstacles," *Russian, Mechatron., Automat., Control*, vol. 22, no. 3, pp. 145–154, 2021.
[18] P. Marantos, Y. Koveos, and K. J. Kyriakopoulos, "UAV state estimation using adaptive complementary filters," *IEEE Trans. Control Syst. Technol.*, vol. 24, no. 4, pp. 1214–1226, Jul. 2016.
[19] R. Mahony, T. Hamel, and J.-M. Pflimlin, "Nonlinear complementary filters on the special orthogonal group," *IEEE Trans. Autom. Control*, vol. 53, no. 5, pp. 1203–1218, Jun. 2008.
[20] T. Hiller, Z. Pentek, J.-T. Liewald, A. Buhmann, and H. Roth, "Origins and mechanisms of bias instability noise in a three-axis mode-matched MEMS gyroscope," *J. Microelectromech. Syst.*, vol. 28, no. 4, pp. 586–596, 2019.
[21] B. Zhou, H. Fang, and J. Xu, "UWB-IMU-odometer fusion localization scheme: Observability analysis and experiments," *IEEE Sensors J.*, vol. 23, no. 3, pp. 2550–2564, Feb. 2023.
[22] X. Tong, M. Chen, and F. Yang, "Passive and explicit attitude and gyro-bias observers using inertial measurements," *IEEE Trans. Ind. Electron.*, vol. 68, no. 9, pp. 8942–8952, Sep. 2021.
[23] S. Rafatnia, H. Nourmohammadi, and J. Keighobadi, "Fuzzy-adaptive constrained data fusion algorithm for indirect centralized integrated SINS/GNSS navigation system," *GPS Solutions*, vol. 23, no. 3, 2019, Art. no. 62.
[24] T. A. Johansen, J. M. Hansen, and T. I. Fossen, "Nonlinear observer for tightly integrated inertial navigation aided by pseudo-range measurements," *J. Dyn. Syst. Meas. Control*, vol. 139, no. 1, 2017, Art. no. 001007.
[25] D. E. Zlotnik and J. R. Forbes, "Nonlinear estimator design on the special orthogonal group using vector measurements directly," *IEEE Trans. Autom. Control*, vol. 62, no. 1, pp. 149–160, Jan. 2017.
[26] H. A. Hashim and A. E. E. Eltoukhy, "Landmark and IMU data fusion: Systematic convergence geometric nonlinear observer for slam and velocity bias," *IEEE Trans. Intell. Transp. Syst.*, vol. 23, no. 4, pp. 3292–3301, Apr. 2022.
[27] S. Berkane and A. Tayebi, "On the design of attitude complementary filters on SO(3)," *IEEE Trans. Autom. Control*, vol. 63, no. 3, pp. 880–887, Mar. 2018.
[28] L. Xiao, L. Li, W. Huang, X. Li, and L. Jia, "A new predefined time zeroing neural network with drop conservatism for matrix flows inversion and its application," *IEEE Trans. Cybern.*, early access, Dec. 13 2022, doi: 10.1109/TCYB.2022.3225155.
[29] M. Brossard, S. Bonnabel, and A. Barrau, "Denoising IMU gyroscopes with deep learning for open-loop attitude estimation," *IEEE Robot. Automat. Lett.*, vol. 5, no. 3, pp. 4796–4803, Jul. 2020.
[30] F. Huang, Z. Wang, L. Xing, and C. Gao, "A MEMS IMU gyroscope calibration method based on deep learning," *IEEE Trans. Instrum. Meas.*, vol. 71, Mar. 22, 2022, Art. no. 1003009.
[31] R. Hamrah, R. R. Warier, and A. K. Sanyal, "Finite-time stable estimator for attitude motion in the presence of bias in angular velocity measurements," *Automatica*, vol. 132, 2021, Art. no. 109815.
[32] S. Han, S. Luo, J. Lu, and J. Dong, "A unified modeling approach of stochastic error in fiber optic gyro and application in INS initial alignment," *IEEE Sensors J.*, vol. 20, no. 13, pp. 7241–7252, Jul. 2020.
[33] J. Guo, Q. Zhang, H. Chai, and Y. Li, "Obtaining lower-body Euler angle time series in an accurate way using depth camera relying on optimized Kinect CNN," *Measurement*, vol. 188, 2022, Art. no. 110461.
[34] Z. Wang et al., "Motion analysis of deadlift for trainers with different levels based on body sensor network," *IEEE Trans. Instrum. Meas.*, vol. 70, Feb. 25, 2021, Art. no. 9506212.

Ning Tang born in 1995, received the B.S. degree in automation science and electrical engineering from Beihang University, Beijing, China, and the M.S. degree in nanoengineering from Bauman Moscow State Technical University, Moscow, Russia, in 2017 and 2020, respectively. He is currently working toward the Ph.D. degree in control science and engineering with Beihang University and Bauman Moscow State Technical University.

Jieling Chang born in 1998, received the B.S. degree in automation science and electrical engineering from Beihang University, Beijing, China, in 2020. He is currently working toward the master degree in control science and engineering with Beihang University.

Lingling Wang received the B.S. and M.S. degrees in automation science from Qufu Normal University, Qufu, China, in 2004 and 2007, respectively, and the Ph.D. degree in control science and engineering from Beihang University, Beijing, China, in 2012.

She is an Associate Professor with the School of Automation Science and Electrical Engineering, Beihang University, where she is one backbone Teacher with the National (Virtual Simulation) Experimental Teaching Demonstration Center of Mechanical and Control Engineering.

Li Fu (Member, IEEE) received the B.S., M.S., and Ph.D. degrees in control science and engineering from Northwestern Polytechnical University, Xi'an, China, in 1991, 1994, and 1997, respectively.

From 2011 to 2012, she was a Visiting Scholar with Purdue University, West Lafayette, IN, USA. She is currently the Director and Professor with the National (Virtual Simulation) Experimental Teaching Demonstration Center of Mechanical and Control Engineering, Beihang University, Beijing, China.

Dr. Fu is also an AIAA member. She was the recipient of the Industry-university-research Innovation Achievement Award for her outstanding contribution to research and teaching. She was the recipient of the NSFC four times since 2010.

Konstantin A. Neusypin received the Ph.D. degree in intelligent control system from Bauman Moscow State Technical University (BMSTU), Moscow, Russia, in 1987, and the degree of doctor of technical science in information processing of navigation systems and aircraft complexes from the Moscow Institute of Electronics and Mathematics, Moscow, Russia, in 1996.

He held the positions as a Research Fellow, Senior Research Fellow, Professor, and the Department Head with Automatic Control Systems, BMSTU.

Dr. Neusypin was the recipient of the prize of the Russian Federation Government in the field of education in 2014 and 2016, respectively.

Maria S. Selezneva received the M.S. and Ph.D. degrees in intelligent navigation systems from Bauman Moscow State Technical University, Moscow, Russia, in 2015 and 2018, respectively.

She is an Associate Professor with the Department of Automatic Control Systems, Bauman Moscow State Technical University since 2018.

Dr. Selezneva was the recipient of the Russian Government Prize in the field of science and technology for young scientists in 2019.

Linping Peng born in 1966, received the Ph.D. degree in mathematics with the School of Mathematical Science, Peking University, Beijing, China, in 1997.

She is a mathematical Professor with Beihang University, Beijing, China. Her research focuses on the qualitative and bifurcation theory of some differential systems, including smooth and nonsmooth systems. She has published some papers about the limit cycles bifurcation of smooth and nonsmooth differential systems. In addition, she also does some research on the application of nonsmooth differential systems in the engineering.